Chemical Science

EDGE ARTICLE

View Article Online
View Journal | View Issue

Cite this: *Chem. Sci.*, 2017, **8**, 8345

Fluorinated Eu^{II}-based multimodal contrast agent for temperature- and redox-responsive magnetic resonance imaging†

Lina A. Basal,[a] Matthew D. Bailey,[a] Jonathan Romero,[b] Meser M. Ali,[c] Lyazat Kurenbekova,[d] Jason Yustein,[de] Robia G. Pautler*[b] and Matthew J. Allen*[a]

Magnetic resonance imaging (MRI) using redox-active, Eu^{II}-containing complexes is one of the most promising techniques for noninvasively imaging hypoxia *in vivo*. In this technique, positive (T_1-weighted) contrast enhancement persists in areas of relatively low oxidizing ability, such as hypoxic tissue. Herein, we describe a fluorinated, Eu^{II}-containing complex in which the redox-active metal is caged by intramolecular interactions. The position of the fluorine atoms enables temperature-responsive contrast enhancement in the reduced form of the contrast agent and detection of the oxidized contrast agent *via* MRI *in vivo*. Positive contrast is observed in ^{1}H-MRI with Eu in the +2 oxidation state, and chemical exchange saturation transfer and ^{19}F-MRI signal are observed with Eu in the +3 oxidation state. Contrast enhancement is controlled by the redox state of Eu, and modulated by the fluorous interactions that cage a bound water molecule reduce relaxivity in a temperature-dependent fashion. Together, these advancements constitute the first report of *in vivo*, redox-responsive imaging using ^{19}F-MRI.

Received 18th July 2017
Accepted 18th October 2017

DOI: 10.1039/c7sc03142d

rsc.li/chemical-science

Introduction

Oxygen is critical to all forms of aerobic life, and imbalances of oxygen supply and consumption, such as hypoxia, are associated with disease.[1–7] For example, hypoxic and nonhypoxic tumors have different responses to therapies, and regions of hypoxic tissue can be extremely heterogenous,[8] complicating the differentiation of different types of tissues. Consequently, many visualization techniques, including optical imaging, positron emission tomography, photoacoustic imaging, and magnetic resonance imaging (MRI), are being investigated for the imaging of oxygen levels to study the progress and treatment of diseases.[9] MRI is capable of producing images of the inside of living organisms with excellent spatial resolution, and ^{19}F has no detectable background signal *in vivo*. As a result of these properties, ^{19}F-MRI has been used *in vivo* with perfluorocarbon emulsions,[10] perfluorocarbon nanoparticles,[11,12] perfluorocarbon-labelled cells,[13,14] and discrete lanthanide complexes.[15] These examples of *in vivo* imaging with ^{19}F-MRI make the technique one of the most promising for noninvasive imaging, and metal-based multimodal oxygen-responsive contrast agents for ^{19}F-MRI would expand that promise to the imaging of hypoxia-related diseases. The design of contrast agents for ^{19}F-MRI is complicated by the conflict between the need for a large number of chemically equivalent fluorine atoms and the hydrophobicity of fluorine. Too few ^{19}F nuclei lead to undetectable signal, but too many ^{19}F nuclei are associated with low solubility.[12] Ideally, oxygen-responsive contrast agents for ^{19}F-MRI would be soluble in water to enable distribution *in vivo* and be redox-responsive to yield molecular information regarding oxidation. Furthermore, because the ^{19}F atoms in ligands are not intrinsically redox-active, redox-responsive probes for ^{19}F-MRI need to include a redox-active element to impart a responsive nature to probes. $Eu^{II/III}$-based contrast agents react with oxygen to change MRI-relevant properties: Eu^{II} enhances contrast in T_1-weighted MRI and Eu^{III} does not.[16–22] We hypothesized that combining the favorable imaging properties of ^{19}F-MRI with ^{1}H-MRI-active Eu^{II}-based complexes would produce oxidation-state-dependent imaging and enable detection of both oxidation states of Eu. We overcame the solubility challenges associated with ^{19}F *via* strategic placement of ^{19}F atoms in ligands for europium that sequestered the fluorine atoms *via* intramolecular interactions. An important consequence of these intramolecular interactions was the formation of a cage that trapped a molecule of water bound to europium, enabling control over contrast enhancement

[a]*Department of Chemistry, Wayne State University, 5101 Cass Avenue, Detroit, Michigan 48202, USA. E-mail: mallen@chem.wayne.edu*

[b]*Department of Molecular Physiology and Biophysics, Baylor College of Medicine, One Baylor Plaza, Houston, Texas 77030, USA. E-mail: rpautler@bcm.edu*

[c]*Department of Neurosurgery, Henry Ford Hospital, 1 Ford Place, Detroit, Michigan 48202, USA*

[d]*Integrative Molecular and Biomedical Sciences, Baylor College of Medicine, Houston, TX 77030, USA*

[e]*Department of Pediatrics, Texas Children's Cancer and Hematology Centers, Baylor College of Medicine, Houston, TX 77030, USA*

† Electronic supplementary information (ESI) available. CCDC 1562330 and 1562331. For ESI and crystallographic data in CIF or other electronic format see DOI: 10.1039/c7sc03142d

in a temperature-responsive manner. Here, we report a new redox-active contrast system, **2Eu$^{II/III}$**, that has twelve chemically equivalent ^{19}F nuclei, is water-soluble, and is detectable *in vivo* before and after oxidation using different imaging protocols with a single MRI scanner.

Our strategy was based upon the ability of Eu^{II}, but not Eu^{III} that has a diamagnetic ground state, to dramatically influence the relaxation rates of nearby nuclei.[17] Although Eu^{III} has low-lying excited paramagnetic electronic states that are thermally accessible, no measurable effect on relaxation rates have been observed at concentrations up to 6 mM.[16,17,19] Eu^{II} is isoelectronic with Gd^{III}, which is commonly used in contrast agents for MRI. Fluorinated Gd^{III}-containing complexes influence the signal of ^{19}F in a distance-dependent manner;[22–28] consequently, we hypothesized that introducing ^{19}F nuclei near Eu^{II} would cause severe line-broadening (*via* shortening of the transverse relaxation time of ^{19}F) to the point of no observable signal. However, unlike Gd^{III} that is not redox-active *in vivo*, oxidation of Eu^{II} to Eu^{III} would be expected to remove quenching of ^{19}F signal. Therefore, Eu-containing complexes would act as T_1-shortening contrast agents for ^{1}H-MRI in the +2 oxidation state and "turn-on" ^{19}F imaging probes in response to oxidation of Eu^{II} to Eu^{III}. Based on recent reports of Eu^{II}-based contrast agents,[16,17,29] we thought that a cyclen scaffold would provide a synthetically viable opportunity to coordinate both oxidation states of Eu near multiple chemically equivalent ^{19}F nuclei while maintaining solubility in water. Our design incorporates twelve equivalent ^{19}F nuclei that enable detection *in vivo* but also provides solubility for clearance *via* the excretory system. Because a single MRI scanner can be used for ^{19}F- and ^{1}H-MRI, the **2Eu$^{II/III}$** system would be detectable before and after oxidation using the same instrument.

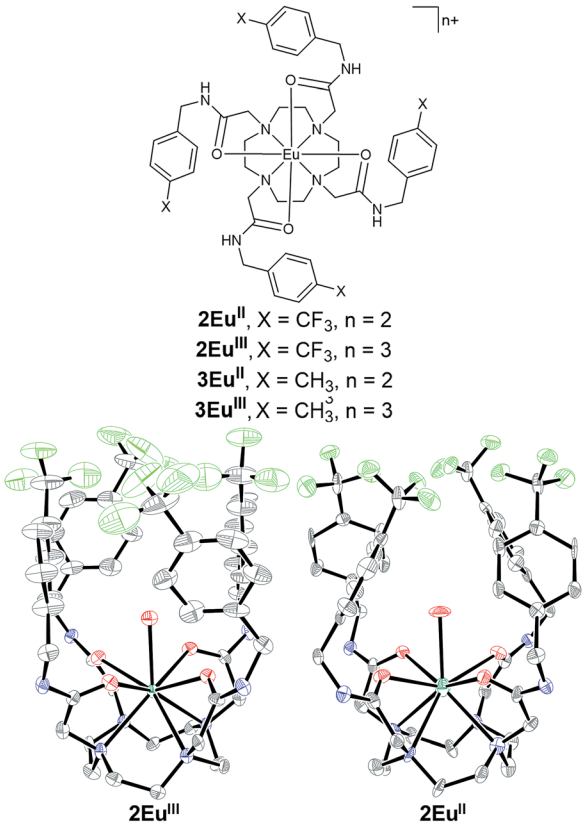

Fig. 1 (Left) Chemical structures of **2Eu^{II}**, **2Eu^{III}**, **3Eu^{II}**, and **3Eu^{III}**. Crystal structures of (center) **2Eu^{II}** and (right) **2Eu^{III}** grown from solutions in methanol and ethanol, respectively. Chloride counterions, outer-sphere water molecules, and hydrogen atoms are not shown for clarity. Thermal ellipsoids are drawn at 50% probability. Grey = C; blue = N; red = O; yellow-green = F; sea green = Eu. Crystallographic data for these structures have been deposited at the Cambridge Crystallographic Data Centre under deposition numbers CCDC 1562330 (**2Eu^{II}**) and CCDC 1562331 (**2Eu^{III}**).†

Results and discussion

Fluorinated ligand **2** was synthesized in two steps from commercially available starting materials (see the ESI† for detailed procedures, yields, and characterization). Ligand **2** was metalated with $EuCl_3$ to produce **2Eu^{III}** (59% yield), and **2Eu^{II}** was synthesized in quantitative yield by reducing **2Eu^{III}** with Zn^0. Complex **2Eu^{III}** can be recovered by oxidizing solutions of **2Eu^{II}** with air as evidenced by UV-visible, ^{19}F-NMR, and luminescence spectroscopies (ESI Fig. S2†). Both **2Eu^{III}** and **2Eu^{II}** are soluble in neutral, buffered water suitable for *in vivo* injections. Furthermore, both complexes share similar conformations in the solid state (Fig. 1). All four amide arms are pseudo-axial, resulting in caged structures around the Eu ions. This conformation is unusual for tetraamide complexes with lanthanides. In all reported examples, amide arms favor pseudo-equatorial positions unless forced to be pseudo-axial by intramolecular steric interactions.[30–32] The structures of **2Eu^{III}** and **2Eu^{II}** suggest that the fluorophilic character of the CF_3 groups and π-stacking of the benzene rings contribute to the formation of a cage around the metal. Additionally, in both **2Eu^{III}** and **2Eu^{II}**, one coordinated water molecule is held within the pocket formed by the *p*-trifluoromethylbenzyl groups, effectively caging the coordinated water molecule from the surroundings. Although trapping of water has implications for T_1-weighted MRI because impeded water exchange influences relaxivity,[33] the pseudo-axial amides could be useful for temperature control of relaxivity. However, crystal structures describe solid-state conformations and do not account for dynamics in solution; therefore, we turned to solution-phase characterization.

To probe the stability of the pseudo-axial conformation in solution, relaxivity was measured as a function of temperature at 11.7 T between 16.5 and 40.5 °C (Fig. 2). This temperature range was selected because it spans from slightly below room temperature to slightly above body temperature. The plot of relaxivity *versus* temperature of **2Eu^{II}** shows two regimes: there is no change in relaxivity between 16.5 and 24.5 °C, and there is a linear increase in relaxation rate between 24.5 and 40.5 °C. The relaxivity at 36.5 °C is 2.0× higher than the relaxivity at 16.5 °C. At the colder temperature, the relaxivity of **2Eu^{II}** is similar to Eu^{II}-containing complexes with purely outer-sphere contrast enhancement (a coordinated water molecule does not measurably influence relaxivity if it is not exchanging with bulk water),[34] and the relaxivity at 36.5 °C is within the range of reported Eu^{II}-containing complexes that have exchanging water.[17,18,34–39] The

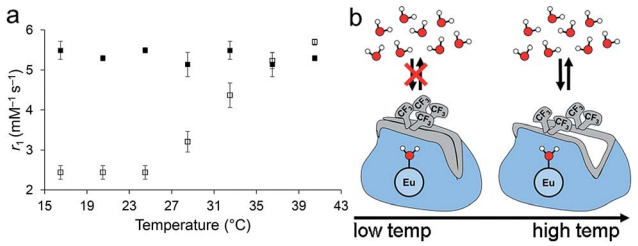

Fig. 2 (a) Relaxation rates (11.7 T) of **2Eu^{II}** (□) (2–8 mM in aqueous 3-morpholinopropane-1-sulfonic acid buffer, pH 7.0) and **3Eu^{II}** (■) (2–15 mM in aqueous 3-morpholinopropane-1-sulfonic acid buffer, pH 7.0). Error bars represent the standard error of mean of measurements from three independently prepared samples. (b) Cartoon explanation of mechanism of temperature-dependent change in relaxivity. The coin purse represents ligand **2** that is held shut by the fluorous interactions and π-stacking at low temperatures, preventing water exchange and, consequently, inner-sphere-based contrast enhancement. As temperature increases, thermal energy overcomes the interactions, opening the ligand to enable water exchange consistent with an increase in relaxivity.

observed dependence on temperature is the opposite of what would be expected for a system that does not change the number of coordinated water molecules: increased temperatures lead to more rapid molecular rotations that are associated with lower relaxivity values.[40] A similar, but smaller, effect in relaxivity caused by hydrophobic groups around a caged water molecule has been previously observed with a structurally similar Gd^{III} complex that has four *N*-(1-phenylethyl)propionamide arms and exhibits a similar increase in relaxivity over the same temperature range.[41,42] Additionally, the change in relaxivity is consistent with Gd^{III}-based responsive contrast agents that modulate water coordination number.[43] A possible explanation for this temperature-dependent shift in relaxivity is that thermal energy overcomes the fluorous and π-stacking interactions above 24.5 °C, resulting in accessibility of bulk water to participate in exchange with the coordinated water inside of the cage formed by the *p*-trifluoromethylbenzyl arms. Conformational changes of similar Eu^{III}- and Gd^{III}-containing, cyclen-based complexes have been reported to influence water-exchange rates.[42,44–47] Finally, to check for the possibility of aggregation, we performed dynamic light scattering measurements of **2Eu^{II}** (3.1 mM in aqueous 3-morpholinopropane-1-sulfonic acid buffer) at 5 and 37 °C: No aggregates were detected at either temperature, supporting a mechanism of relaxivity modulation based on water exchange instead of molecular reorientation. The observed changes in relaxivity are consistent with what would be expected if pseudo-axial amides in the solid-state structure were similar to solution-phase at lower temperatures, and thermal energy at higher temperatures overcame intramolecular fluorous interactions to enable water exchange.

To explore the influence of the fluorous interactions between the trifluoromethyl moieties on the temperature-dependent behavior of **2Eu^{II}**, we synthesized the nonfluorinated methyl analog, **3Eu^{II}**, and measured relaxivity over the same range of temperatures. Ligand **3** was synthesized in two steps from commercially available starting materials, and the corresponding Eu-containing complexes, **3Eu^{III}** and **3Eu^{II}**, were synthesized similarly to **2Eu^{III}** and **2Eu^{II}** (ESI Fig. S1†). The methylated complex, **3Eu^{II}**, did not exhibit a temperature-dependent change in relaxivity like the fluorinated complex **2Eu^{II}**. Between 16.5 and 36.5 °C, **3Eu^{II}** displayed relaxivities from 5.14 to 5.49 mM^{-1} s^{-1}, similar to the relaxivity of the trifluoromethyl complex, **2Eu^{II}**, at temperatures ≥36.5 °C. The lack of temperature dependence of the methyl analog **3Eu^{II}** suggests that intramolecular fluorous interactions are the cause of the temperature-dependent relaxivity of **2Eu^{II}**. Therefore, the fluorous interactions impart an element of kinetic control that has implications for long-term storage and could be used to measure temperature using relaxivity.

To test if the *p*-trifluoromethylbenzylamide arms would enable detection after oxidation of Eu^{II} to Eu^{III}, we studied the spectroscopic properties of **2Eu$^{II/III}$**. To verify that the ^{19}F-NMR signal changes with oxidation state, we acquired ^{19}F-NMR spectra of aqueous, buffered solutions of **2Eu^{III}** and **2Eu^{II}** (5.4 mM in aqueous 3-morpholinopropane-1-sulfonic acid buffer, pH 7.0). A singlet at −62.1 ppm relative to sodium triflate was observed for **2Eu^{III}**, and no detectable signal was observed for **2Eu^{II}**. Upon oxidation of the solution of **2Eu^{II}**, ^{19}F-signal appeared consistent with the presence of **2Eu^{III}** (ESI Fig. S2†). The ^{19}F-NMR signal was too broad to be observed for **2Eu^{II}** because the Eu^{II} ion shortened the transverse relaxation times of ^{19}F to the point of no observable signal. Upon oxidation to Eu^{III}, ^{19}F signal appeared. Furthermore, because not all MRI scanners are capable of imaging ^{19}F, we also acquired the chemical exchange saturation transfer (CEST) spectrum of **2Eu^{III}**. Amides near Eu^{III} and Eu^{II} provide a means of imaging oxygen content *via* CEST MRI.[17] Complex **2Eu^{III}** has a saturation offset of 49 ppm (ESI Fig. S3†), which is similar to other Eu^{III}-containing tetraamide complexes.[17,30,31,48,49] Therefore, based on spectroscopic studies, **2Eu^{III}** has detectable ^{19}F- and CEST MRI after oxidation.

To verify that the oxidation-state-dependent signal was observable with MRI at imaging-relevant concentrations, we imaged solutions of complexes **2Eu^{III}**, **2Eu^{II}**, and **2Eu^{III}** post-oxidation (Fig. 3). ^{19}F- and CEST-MRI signals were observed for Eu^{III}-containing complex **2Eu^{III}**, but no T_1-weighted enhancement was observed relative to buffer. No detectable ^{19}F- or CEST-MRI signals were observed for Eu^{II}-containing complex **2Eu^{II}**, but a 2.0× increase in brightness in the T_1-weighted scan was observed relative to buffer (see ESI Fig. S8 and Table S4† for signal-to-noise ratios). This observation is consistent with another Eu^{II}-containing tetraamide complex without benzyl groups that does not influence CEST-MRI but does shorten T_1.[17] Therefore, the pair of complexes, **2Eu^{II}** and **2Eu^{III}**, provide oxidation-dependent signal: the Eu^{II}-containing complex acts as a T_1-enhancing contrast agent, and the Eu^{III}-containing complex acts as an imaging probe for ^{19}F- and CEST-MRI. Due to the well-behaved redox- and temperature-responsive contrast system **2Eu$^{II/III}$** *in vitro*, we investigated the behavior of the system in mice.

To verify that oxidation-state-dependent signals were observable with MRI *in vivo*, mice were injected in the peritoneal cavities with solutions of **2Eu^{II}** (200 μL, 5.4 mM in aqueous 3-morpholinopropane-1-sulfonic acid buffer, pH 7.0) and imaged with T_1-weighted and ^{19}F-MRI scans (Fig. 4a–e). All animal studies were done in accordance with protocols preapproved by

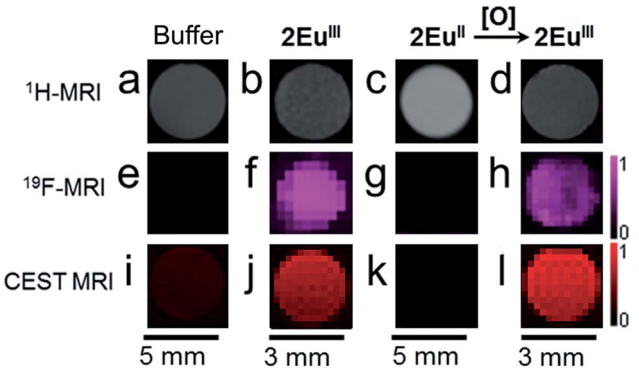

Fig. 3 MR images of solutions of samples in aqueous 3-morpholinopropane-1-sulfonic acid buffer (20 mM, pH 7.0) in glass (3 mm) or plastic tubes (5 mm). Scale bars correspond to the three images in the column above each bar. T_1-weighted MRI images of solutions of (a) 3-morpholinopropane-1-sulfonic acid (20 mM, pH 7.0) (b) **2Eu^{III}** (3.5 mM); (c) **2Eu^{II}** (3.5 mM); and (d) **2Eu^{III}** after oxidation of **2Eu^{II}** (3.5 mM). ^{19}F-MRI images of (e) 3-morpholinopropane-1-sulfonic acid (20 mM, pH 7.0); (f) **2Eu^{III}** (3.5 mM); (g) **2Eu^{II}** (3.5 mM); and (h) **2Eu^{III}** after oxidation of **2Eu^{II}** (3.5 mM). The scale bar on the right of (h) represents signal intensity for all ^{19}F- MRI images in Fig. 3. CEST MRI images of (i) 3-morpholinopropane-1-sulfonic acid (20 mM, pH 7.0); (j) **2Eu^{III}** (3.5 mM); (k) **2Eu^{II}** (3.5 mM); and (l) **2Eu^{III}** after oxidation of **2Eu^{II}** (3.5 mM). The scale bar on the right of (l) represents signal intensity for all CEST MRI images in Fig. 3.

the Institutional Animal Care and Use Committee of Baylor College of Medicine. Intraperitoneal injections were selected to enable comparison with previous Eu^{II} studies.[20] Because intraperitoneal injections in a normal mouse are in non-hypoxic conditions, it is expected that the contrast agent would lose T_1 contrast and develop ^{19}F signal intensity upon oxidation. T_1-weighted MRI images of the coronal planes of mice showed contrast that appeared immediately upon injection and faded over the course of three minutes. The duration of T_1-enhancement is consistent with intraperitoneal injection of a Eu^{II}-containing cryptate.[20] To detect **2Eu^{III}** post-oxidation *in vivo*, we collected ^{19}F spectra of mice between T_1-weighted scans. ^{19}F signal intensity appeared nine minutes post injection (Fig. 4i). The *in vivo* ^{19}F spectra demonstrated that **2Eu^{III}** could be detected post-oxidation *in vivo* using a ^{19}F coil of an MRI scanner. Other ^{19}F-MRI, redox-responsive contrast agents have been demonstrated to display oxidation-dependent signal *in vitro* or *ex vivo*,[50–53] but to the best of our knowledge, this is the first demonstration of detection of ^{19}F-MR signal *in vivo* in a redox-responsive manner.

Encouraged by the T_1 and ^{19}F oxidation-response *in vivo*, we investigated the *in vivo* solubility and clearance by collecting a sample of urine after imaging and within one hour of injection. The urine was analyzed using coupled high-performance liquid chromatography mass spectrometry. The $[M + Cl]^{2+}$ adduct of **2Eu^{III}** was observed with the correct mass-to-charge ratio and expected isotope pattern (ESI Fig. S4†). Although this technique is not quantitative, evidence of intact complex post-injection is promising for future *in vivo* studies with respect to minimization of toxicity from decomplexation or transmetallation.[54] Furthermore, evidence of intact complex indicates that **2Eu$^{II/III}$** remained soluble, diffused through the mouse, and was cleared intact.

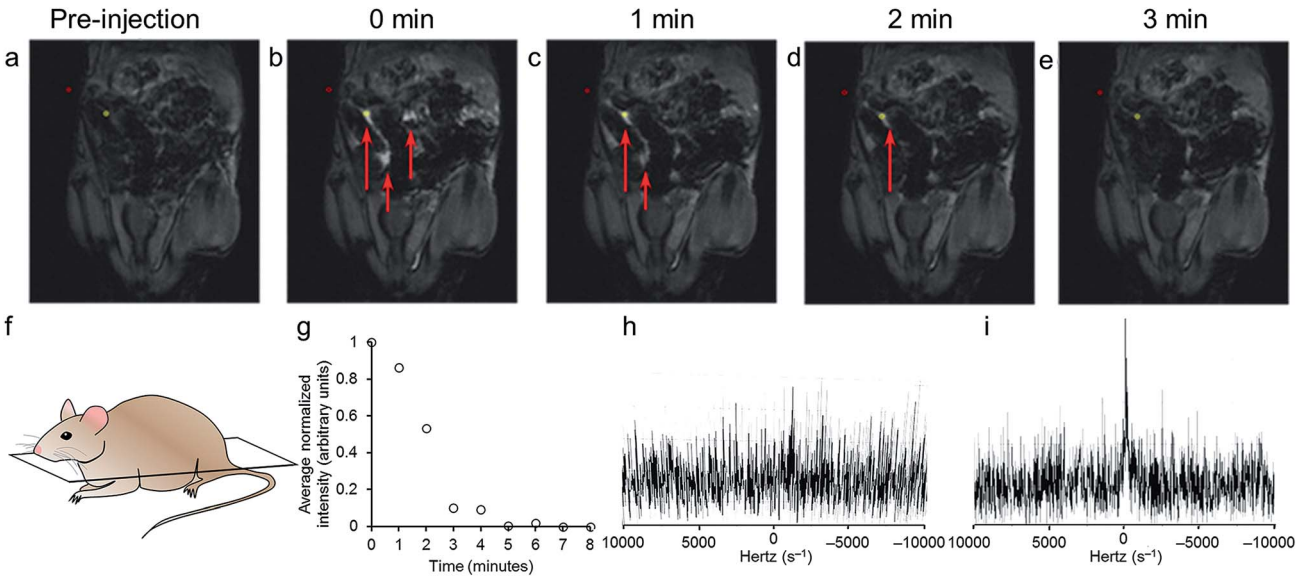

Fig. 4 Representative T_1-weighted images demonstrating the response of **2Eu^{II}** (5.4 mM in aqueous 3-morpholinopropane-1-sulfonic acid buffer, pH 7.0) after intraperitoneal injection (into a 20 g C57/Bl6 mouse). The images are (a) pre-injection, (b) immediately post-intraperitoneal injection, denoted as 0 min, (c) 1 min post-intraperitoneal injection, (d) 2 min post-intraperitoneal injection, and (e) 3 min post-intraperitoneal injection. Red arrows denote areas of positive contrast enhancement. The area represented by each image is 26 mm × 40 mm. (f) Diagram showing plane of the mouse in images a–e. (g) Average normalized pixel brightness, which were subtracted with the pre-injection image intensities, plotted over time post-intraperitoneal injection from panels (a)–(e), the area from the red circles (background) was subtracted from the area in the yellow circles to calculate average pixel brightness. Single pulse ^{19}F signal intensity of a whole mouse (h) pre-injection and (i) nine minutes post-injection.

Conclusions

In conclusion, we have synthesized a new redox-active contrast agent, **2Eu$^{II/III}$**, that also displays temperature-dependent relaxivity, which was used as a tool for probing mechanism. The intramolecular fluorous interactions among *p*-trifluoromethylbenzylamides lead to the formation of a cage-like structure that modulates the interactions of water with Eu as a function of temperature, evidenced by the change in relaxivity. Because of the presence of fluorine atoms and amide protons, the system can be tracked *in vivo* after oxidation with a variety of instruments that are equipped with either CEST or ^{19}F-MR imaging capabilities. We also observed intact complex in mouse urine post-injection, which is promising for future toxicity studies and *in vivo* imaging. Together, our results allude to a new molecular strategy for rationally designing ligand architectures by modulating interactions between Eu^{II} and water with intramolecular fluorous attractions. These results could pave the way to using existing imaging techniques with new chemical agents to access previously unattainable oxidative information noninvasively *in vivo*.

Conflicts of interest

There are no conflicts to declare.

Acknowledgements

The authors acknowledge the National Institutes of Health for support (R01EB013663). L. A. B. is thankful for a Chemical Biology Interface research experience award (Wayne State University). We thank Kyle Blakeney, Levi Ekanger, and Michael Pirrone for technical assistance and helpful discussions. We thank the Small Animal Imaging Facility, Texas Children's Hospital, Houston, TX, and Baylor College of Medicine Small Animal MRI ATC, Houston, TX, for use of their imaging facility.

References

1 A. Facciabene, X. Peng, I. S. Hagemann, K. Balint, A. Barchetti, L.-P. Wang, P. A. Gimotty, C. B. Gilks, P. Lal, L. Zhang and G. Coukos, *Nature*, 2011, **475**, 226.
2 K. Ishikawa, K. Takenaga, M. Akimoto, N. Koshikawa, A. Yamaguchi, H. Imanishi, K. Nakada, Y. Honma and J.-I. Hayashi, *Science*, 2008, **320**, 661.
3 D. Shweiki, A. Itin, D. Soffer and E. Keshet, *Nature*, 1992, **359**, 843.
4 L. Park, P. Zhou, R. Pitstick, C. Capone, J. Anrather, E. H. Norris, L. Younkin, S. Younkin, G. Carlson, B. S. McEwen and C. Iadecola, *Proc. Natl. Acad. Sci. U. S. A.*, 2008, **105**, 1347.
5 M. P. Mattson, *Nature*, 2004, **430**, 631.
6 M. T. Lin and M. F. Beal, *Nature*, 2006, **443**, 787.
7 K. J. Barnham, C. L. Masters and A. I. Bush, *Nature Reviews*, 2004, **3**, 205.
8 M. Jamal-Hanjani, S. A. Quezada, J. Larkin and C. Swanton, *Clin. Cancer Res.*, 2015, **21**, 1258.
9 J. Liu, W. Bu and J. Shi, *Chem. Rev.*, 2017, **117**, 6160.
10 R. P. Mason, W. Rodbumrung and P. Antich, *NMR Biomed.*, 1996, **9**, 125.
11 H. Matsushita, S. Mizukami, F. Sugihara, Y. Nakanishi, Y. Yoshioka and K. Kikuchi, *Angew. Chem., Int. Ed.*, 2014, **53**, 1008.
12 R. Díaz-López, N. Tsapis and E. Fattal, *Pharm. Res.*, 2009, **27**, 1.
13 M. Srinivas, P. A. Morel, L. A. Ernst, D. H. Laidlaw and E. T. Ahrens, *Magn. Reson. Med.*, 2007, **58**, 725.
14 E. T. Ahrens, R. Flores, H. Xu and P. A. Morel, *Nat. Biotechnol.*, 2005, **23**, 983.
15 E. De Luca, P. Harvey, K. H. Chalmers, A. Mishra, P. K. Senanayake, J. I. Wilson, M. Botta, M. Fekete, A. M. Blamire and D. Parker, *J. Biol. Inorg. Chem.*, 2014, **19**, 215.
16 L. A. Basal, Y. Yan, Y. Shen, E. M. Haacke, M. Mehrmohammadi and M. J. Allen, *ACS Omega*, 2017, **2**, 800.
17 L. A. Ekanger, D. R. Mills, M. M. Ali, L. A. Polin, Y. Shen, E. M. Haacke and M. J. Allen, *Inorg. Chem.*, 2016, **55**, 9981.
18 P. Caravan, É. Tóth, A. Rockenbauer and A. E. Merbach, *J. Am. Chem. Soc.*, 1999, **121**, 10403.
19 L. A. Ekanger, M. M. Ali and M. J. Allen, *Chem. Commun.*, 2014, **50**, 14835.
20 L. A. Ekanger, L. A. Polin, Y. Shen, E. M. Haacke and M. J. Allen, *Contrast Media Mol. Imaging*, 2016, **11**, 299.
21 L. A. Ekanger, L. A. Polin, Y. Shen, E. M. Haacke, P. D. Martin and M. J. Allen, *Angew. Chem., Int. Ed.*, 2015, **54**, 14398.
22 C. U. Lenora, F. Carniato, Y. Shen, Z. Latif, E. M. Haacke, P. D. Martin, M. Botta and M. J. Allen, *Chem.–Eur. J.*, 2017, DOI: 10.1002/chem.201702158.
23 S. Mizukami, R. Takikawa, F. Sugihara, Y. Hori, H. Tochio, M. Wälchli, M. Shirakawa and K. Kikuchi, *J. Am. Chem. Soc.*, 2008, **130**, 794.
24 T. Nakamura, H. Matsushita, F. Sugihara, Y. Yoshioka, S. Mizukami and K. Kikuchi, *Angew. Chem., Int. Ed.*, 2015, **54**, 1007.
25 A. Keliris, I. Mamedov, G. E. Hagberg, N. K. Logothetis, K. Scheffler and J. Engelmann, *Contrast Media Mol. Imaging*, 2012, **7**, 478.
26 T. Sakamoto, Y.-k. Shimizu, J. Sasaki, H. Hayakawa and K. Fujimoto, *Bioorg. Med. Chem. Lett.*, 2011, **21**, 303.
27 X. Yue, Z. Wang, L. Zhu, Y. Wang, C. Qian, Y. Ma, D. O. Kiesewetter, G. Niu and X. Chen, *Mol. Pharmaceutics*, 2014, **11**, 4208.
28 K. Srivastava, E. A. Weitz, K. L. Peterson, M. Marjańska and V. C. Pierre, *Inorg. Chem.*, 2017, **56**, 1546.
29 L. A. Ekanger, L. A. Basal and M. J. Allen, *Chem.–Eur. J.*, 2017, **23**, 1145.
30 J. R. Slack and M. Woods, *J. Biol. Inorg Chem.*, 2014, **19**, 173.
31 T. Mani, A. C. L. Opina, P. Zhao, O. M. Evbuomwan, N. Milburn, G. Tircsó, C. Kumas and A. D. Sherry, *J. Biol. Inorg Chem.*, 2014, **19**, 161.
32 T. Mani, G. Tircso, P. Zhao, A. D. Sherry and M. Woods, *Inorg. Chem.*, 2009, **48**, 10338.

33 B. N. Siriwardena-Mahanama and M. J. Allen, *Molecules*, 2013, **18**, 9352.
34 L. Burai, É. Tóth, S. Seibig, R. Scopelliti and A. E. Merbach, *Chem.–Eur. J.*, 2000, **6**, 3761.
35 J. Garcia and M. J. Allen, *Inorg. Chim. Acta*, 2012, **393**, 324.
36 J. Garcia, A. N. W. Kuda-Wedagedara and M. J. Allen, *Eur. J. Inorg. Chem.*, 2012, 2135.
37 J. Garcia, J. Neelavalli, E. M. Haacke and M. J. Allen, *Chem. Commun.*, 2011, **47**, 12858.
38 L. Burai, R. Scopelliti and É. Tóth, *Chem. Commun.*, 2002, 2366.
39 L. Burai, É. Tóth, G. Moreau, A. Sour, R. Scopelliti and A. E. Merbach, *Chem.–Eur. J.*, 2003, **9**, 1394.
40 P. Caravan, J. J. Ellison, T. J. McMurry and R. B. Lauffer, *Chem. Rev.*, 1999, **99**, 2293.
41 K. H. Chalmers, E. De Luca, N. H. M. Hogg, A. M. Kenwright, I. Kuprov, D. Parker, M. Botta, J. I. Wilson and A. M. Blamire, *Chem.–Eur. J.*, 2010, **16**, 134.
42 A. L. Thompson, D. Parker, D. A. Fulton, J. A. K. Howard, S. U. Pandya, H. Puschmann, K. Senanayake, P. A. Stenson, A. Badari, M. Botta, S. Avedano and S. Aime, *Dalton Trans.*, 2006, 5605.
43 L. M. Matosziuk, J. H. Leibowitz, M. C. Heffern, K. W. MacRenaris, M. A. Ratner and T. J. Meade, *Inorg. Chem.*, 2013, **52**, 12250.
44 S. Aime, A. Barge, M. Botta, A. S. De Sousa and D. Parker, *Angew. Chem., Int. Ed.*, 1998, **37**, 2673.
45 S. Aime, A. Barge, J. I. Bruce, M. Botta, J. A. K. Howard, J. M. Moloney, D. Parker, A. S. de Sousa, D. Parker and M. Woods, *J. Am. Chem. Soc.*, 1999, **121**, 5762.
46 R. S. Dickins, J. A. K. Howard, C. W. Lehmann, J. Moloney, D. Parker and R. Peacock, *Angew. Chem., Int. Ed.*, 1997, **36**, 521.
47 R. S. Dickins, J. A. K. Howard, C. L. Maupin, J. M. Moloney, D. Parker, J. P. Riehl, G. Siligardi and J. A. G. Williams, *Chem.–Eur. J.*, 1999, **5**, 1095.
48 O. M. Evbuomwan, J. Lee, M. Woods and A. D. Sherry, *Inorg. Chem.*, 2014, **53**, 10012.
49 S. Viswanathan, S. J. Ratnakar, K. N. Green, Z. Kovacs, L. M. De León-Rodríguez and A. D. Sherry, *Angew. Chem., Int. Ed.*, 2009, **121**, 9494.
50 D. Xie, T. L. King, A. Banerjee, V. Kohli and E. L. Que, *J. Am. Chem. Soc.*, 2016, **138**, 2937.
51 D. Xie, S. Kim, V. Kohli, A. Banerjee, M. Yu, J. S. Enriquez, J. J. Luci and E. L. Que, *Inorg. Chem.*, 2017, **56**, 6429.
52 K. Tanabe, H. Harada, M. Narazaki, K. Tanaka, K. Inafuku, H. Komatsu, T. Ito, H. Yamada, Y. Chujo, T. Matsuda, M. Hiraoka and S.-i. Nishimoto, *J. Am. Chem. Soc.*, 2009, **131**, 15982.
53 M. Yu, D. Xie, K. P. Phan, J. S. Enriquez, J. J. Luci and E. L. Que, *Chem. Commun.*, 2016, **52**, 13885.
54 J.-M. Idée, M. Port, I. Raynal, M. Schaefer, S. Le Greneur and C. Corot, *Fundam. Clin. Pharmacol.*, 2006, **20**, 563.